

Article

# Waterborne Coating Binders Based on Self-Crosslinking Acrylic Latex with Embedded Inorganic Nanoparticles: A Comparison of Nanostructured ZnO and MgO as Crosslink Density Enhancing Agents

Jana Machotová <sup>1,\*</sup>, Andréa Kalendová <sup>1</sup>, Barbora Zlámaná <sup>1</sup>, Jaromír Šňupárek <sup>1</sup>, Jiří Palarčík <sup>2</sup> and Roman Svoboda <sup>3</sup> 

<sup>1</sup> Institute of Chemistry and Technology of Macromolecular Materials, Faculty of Chemical Technology, University of Pardubice, 532 10 Pardubice, Czech Republic; andrea.kalendova@upce.cz (A.K.); bar.zl@seznam.cz (B.Z.); jaromir.snuparek@upce.cz (J.Š.)

<sup>2</sup> Institute of Environmental and Chemical Engineering, Faculty of Chemical Technology, University of Pardubice, 532 10 Pardubice, Czech Republic; jiri.palarcik@upce.cz

<sup>3</sup> Department of Physical Chemistry, Faculty of Chemical Technology, University of Pardubice, 532 10 Pardubice, Czech Republic; roamn.svoboda@upce.cz

\* Correspondence: jana.machotova@upce.cz; Tel.: +420-466-037-194

Received: 26 February 2020; Accepted: 27 March 2020; Published: 1 April 2020



**Abstract:** This paper is focused on a simple preparation of functional acrylic latex coating binders comprising embedded nanoparticles originating from ZnO and MgO, respectively, in the role of interfacial ionic self-crosslinking agents. The incorporation of surface-untreated powdered nano-oxides into the coating binder was achieved in the course of the latex synthesis performed by a technique of the two-step emulsion polymerization. By means of this technological approach, latexes comprising dispersed nanoparticles in the content of ca 0.5–1.1 wt % (based on solids) were successfully prepared. For the interfacial covalent self-crosslinking, diacetone acrylamide repeat units were introduced into the latex polymer to ensure functionalities for the subsequent reaction with adipic acid dihydrazide. The latex storage stability and coating performance were compared with respect to the type and concentration of the incorporated nanoparticles. It was determined that all latex coating binders comprising nanoparticles exhibited long-term storage stability and provided interfacially crosslinked transparent smooth coating films of high gloss, excellent solvent resistance, and favorable physico-mechanical properties. Moreover, latexes with embedded nanoparticles, which originated from MgO, manifested a pronounced drop in minimum film forming temperature and provided highly water whitening resistant coating films.

**Keywords:** self-crosslinking latex; ionic crosslinking; nanoparticle; zinc oxide; magnesium oxide

## 1. Introduction

With increasing demand for eco-friendly waterborne coatings, aqueous polymer dispersions—so-called latexes—are of a particular practical importance. In spite of their increasing popularity, the typical shortcomings of latex coatings, such as water sensitivity, low solvent resistance, and unfavorable mechanical properties often limit their application. To overcome some of these drawbacks, chemical crosslinking through covalent crosslinking has been a traditionally used tool [1–3]. Among various covalent crosslinking reactions, self-crosslinking using the reaction between carbonyl and hydrazide functionalities from copolymerized diacetone acrylamide (DAAM) and adipic acid dihydrazide

(ADH), respectively, has been the subject of increased interest [4–6]. Adipic acid dihydrazide is dissolved in the latex aqueous medium, thus latexes using the keto-hydrazide crosslinking offer the advantage of a one-component composition with fast interfacial crosslinking at an ambient temperature [7–9].

Apart from the covalent interfacial crosslinking, the improved properties of latex coatings can be obtained by interfacial self-crosslinking through ionic bonding. In the case of carboxylic groups containing latexes, the ionic bonds are usually created in the presence of salts and oxides of multivalent metals [10]. Among these compounds, ZnO—typically in the form of small particles dispersed in aqueous medium—has been used as an effective crosslinking agent providing ambient temperature self-crosslinking of latex coatings [11,12]. Although ZnO is sparingly soluble in water (a few ppm), it has been determined that it neutralizes carboxylated latexes in the wet state and cures them upon drying. Combined with covalent crosslinking, ionic self-crosslinking is referred to impart non-blocking resistance, hardness, adhesion, water, and solvent resistance [13–15].

In recent years, nano-sized ZnO—as one of the multifunctional inorganic nanoparticles—has met with considerable interest in the field of polymer coatings [16–18] due to significant improvement of physical and chemical properties, such as high chemical stability, antimicrobial activity [19,20], photocatalytic activity [21], and intense ultraviolet absorption [22]. Also, in the research area of standard emulsion polymerization, several papers have reported on ZnO nanoparticles embedded into latex polymers [23–28]. Nevertheless, a serious drawback of ZnO is the toxicity for the aquatic environment [29,30]. Moreover, the latest studies concerning ZnO nanoparticle toxicity have revealed toxic effects on rats and potential harmful effects on mammalian cells [31–36]. Efforts to decrease the concentration of nano-sized ZnO in commercial products by its replacement with effective alternatives are therefore being highly encouraged. Among the suitable alternatives, MgO is a promising candidate. In medicine, MgO is used for bone regeneration, treatment of heartburn and a sore stomach [37]. Recently, nano-sized MgO has shown to be a promising remedy in the treatment of tumors [38] and an effective biocide against Gram-positive and Gram-negative bacteria [39]. Nano-sized MgO has been generally considered as a safe material to humans and animals, although its toxicological potential is of concern and safe exposure levels should be assessed. The latest studies mentioned genotoxic potential at high dose levels of MgO nanoparticles on rats and toxic effects on early developmental stages of zebrafish embryos [40,41]. To the best of our knowledge, no papers dealing with latex materials utilizing MgO nanoparticles have been referred to in the relevant literature. MgO nanoparticles have therefore attracted our attention as an effective substitute for nano-sized ZnO in latex coating materials.

In this paper, we report on the preparation and properties of acrylic latexes using the combination of ambient temperature covalent and ionic self-crosslinking. Nano-sized ZnO and MgO, respectively, were used in the role of ionic interfacial self-crosslinking agents. The incorporation of surface-untreated nano-oxides into the latexes was carried out in the course of the latex synthesis performed by a technique of the two-step emulsion polymerization. On the one hand, we were interested in comparing both types of inorganic nano-oxides from the point of view of final coating properties and on the other hand, we wanted to present a facile synthetic route for a harmless and environmentally friendly functional polymer coating binder.

## 2. Materials and Methods

### 2.1. Materials

Latexes were synthesized of methyl methacrylate (MMA), butyl acrylate (BA), methacrylic acid (MAA), and diacetone acrylamide (DAAM). All the monomers were obtained from Sigma-Aldrich (Prague, Czech Republic). Disponil FES 993 (BASF, Prague, Czech Republic) was utilized as the surfactant and ammonium persulfate (Penta, Prague, Czech Republic) was used as the initiator. Adipic acid dihydrazide (ADH) was used as the covalent crosslinker and was received from Sigma-Aldrich. Nano-sized ZnO without any surface modification, having an average particle size below 100 nm, was obtained from Sigma-Aldrich. Surface-unmodified MgO nanoparticles

(trade name JR-NMg30), with a particle size below 200 nm, were received from Xuancheng Jingrui New Materials Co. (Xuancheng, Anhui, China). All the chemicals were utilized as received without any further purification.

## 2.2. Synthesis and Characterization of Latexes

Two series of acrylic latexes, differing in type and content of inorganic nanoparticles (colloidally dispersed in the aqueous phase of polymer dispersion), were prepared by a two-step non-seeded emulsion polymerization technique. To provide the interfacial covalent self-crosslinking, a constant amount of DAAM (5 wt % with respect to second step monomer feeds, which is a typical content of self-crosslinking latex compositions [5,42,43]) was incorporated into the second step polymer to introduce ketone carbonyl functional groups. Carboxylic functionalities (in a relatively high amount) were incorporated into the first and second step polymers by copolymerizing MAA for three reasons: firstly, to enable the ionic interfacial self-crosslinking in the presence of metal oxides; secondly, to assure acidic catalysis of the keto-hydrazide covalent self-crosslinking; and thirdly, to provide the colloidal stability of latexes. The latex sample labeled  $L_0$  represented the reference and did not comprise inorganic nanoparticles, whereas the samples labeled  $L_{ZnO}$  and  $L_{MgO}$  were prepared using different amounts of nanostructured ZnO and MgO, respectively, namely 0, 0.5, 1, 1.5, and 2 wt % (percentage of inorganic nanoparticles added with respect to the total polymer mass present) to provide varying levels of ionic self-crosslinking. The proportions of individual monomers were adjusted to obtain the resulting polymer having a calculated glass transition temperature ( $T_g$ ) of approximately 15 °C (using the Fox equation [44]), so that high-quality film-formation on the one hand and non-tackiness of coatings on the other hand were achieved. The specific proportions of the particular monomers were as follows: 42 g MMA, 53 g BA, and 5 g MAA polymerized in the first step and 41 g MMA, 52 g BA, 2 g MAA, and 5 g DAAM polymerized in the second step. The reduced content of MAA in the second step polymer (in contrast to the first step polymer) was designed to prevent dosing difficulties due to premature ionic bonding in monomer emulsion comprising a particular nano-sized oxide.

The latexes were synthesized in a 1000 mL glass reaction vessel under a nitrogen atmosphere at a polymerization temperature of 85 °C. The reactor charge (consisting of distilled water, surfactant, and initiator, see Table 1) was placed into the reaction vessel and heated to 85 °C. The monomer emulsion was consequently dosed into the stirred reaction vessel at a dosing rate of about 2 mL/min in two steps, while a 15 min-long period between the two dosing steps was held. The polymerization was then completed, during the 2 h of the hold period. A detailed composition of polymerization system is presented in Table 1.

**Table 1.** Composition of polymerization system.

	Reactor Charge (g)	First Step Monomer Emulsion (g)	Second Step Monomer Emulsion (g)
Water	70	75	125
Disponil FES 993	0.5	7.4	7.4
Ammonium persulfate	0.4	0.4	0.4
Monomer mixture	–	100	100
Inorganic nanoparticles	–	–	0–4

For the preparation of the first series of latexes with ZnO nanoparticles, the above described procedure involved the preparation of a finely dispersed ZnO aqueous suspension. ZnO nanopowder was added to water which was designated for the preparation of second step monomer emulsion. (Latexes labelled  $L_{ZnO-0.5}$ ,  $L_{ZnO-1.0}$ ,  $L_{ZnO-1.5}$ , and  $L_{ZnO-2.0}$  were prepared by incorporating ZnO nanopowder in an amount of 1, 2, 3, and 4 g, respectively.) To facilitate the fragmentation of aggregates of ZnO primary nanoparticles, a proper dispersion process using an ULTRA-TURRAX T25 disperser (IKA, Staufen, Germany) at 14,000 rpm was carried out for 20 min followed by 1 h-long

ultra-sonication. The nano-sized ZnO aqueous suspension was then mixed with monomers, emulsifier and initiator designed for the preparation of second step monomer emulsion (using a stirrer at low speed for 3 min). In the end, the resulting second step monomer emulsion comprising nano-sized ZnO nanoparticles, was dosed to the reactor immediately.

For the preparation of the second series of latexes containing MgO nanoparticles, the above-mentioned procedure included the preparation of well-dispersed MgO monomer suspension. Firstly, MgO nanopowder was mixed with monomers (except MAA and DAAM) which were designated for the preparation of second step monomer emulsion. The preparation of latex samples labelled  $L_{MgO-0.5}$ ,  $L_{MgO-1.0}$ ,  $L_{MgO-1.5}$ , and  $L_{MgO-2.0}$  involved the incorporation of nano-MgO in the amount of 1, 2, 3, and 4 g, respectively. First, a proper dispersion process using a SilentCrusher M disperser (Heidolph, Schwabach, Germany) at 15,000 rpm was carried out for 20 min while cooling in an ice bath. The fine nano-MgO monomeric suspension was then mixed with water, emulsifier, initiator, and the rest of the monomers (DAAM and MAA) designed for the preparation of the second step monomer emulsion (using a stirrer at low speed for 3 min). In the end, the resulting second step monomer emulsion with nano-sized MgO was dosed to the reactor immediately.

After the synthesis, the filterable solids were dried and weighed and the coagulum content was calculated according to

$$\text{Coagulum content (\%)} = \frac{100 \times M_f}{\text{real solids content} \times M_E + M_f} \quad (1)$$

where  $M_f$  and  $M_E$  are the weights of dried filterable solids and the filtered emulsion, respectively. The latex pH was consequently adjusted to 8.5 with ammonia solution (in the case of the latexes having their original pH below 8.5). pH testing was performed at  $23 \pm 1$  °C using a pH meter FiveEasy FE20 (Mettler-Toledo, Greifensee, Switzerland). Finally, a 10 wt % aqueous solution of ADH in a content corresponding to the molar ratio ADH:DAAM = 1:2, was added to the latex. Thus, the self-crosslinking latex binders having a solids content of about 42 wt % were prepared. The minimum film-forming temperatures (MFFT) of the self-crosslinking latex binders were determined according to ISO 2115, using the MFFT-60 instrument (Rhopoint Instruments, St Leonards, UK).

### 2.3. Characterization of Inherent Structure of Coating Binder Materials

The structure of the prepared coating binders with the emphasis on the nature of the embedded inorganic nanoparticles and emulsion polymer was investigated using several testing methods. The effect of polymerization reactants and conditions on the chemical nature of the embedded inorganic nanoparticles which originated from the inorganic oxide was estimated by means of an X-ray diffraction (XRD) spectroscopy on a D8-Advance (Bruker AXS, Karlsruhe, Germany) diffractometer with Bragg–Brentano  $\theta$ – $\theta$  geometry using Cu K $\alpha$  radiation. XRD measurements were performed at room temperature (RT) from 5 to 70° (2 $\theta$ ) in 0.02° steps with a counting time of 3 s per step.

The inorganic nanoparticles were also investigated by means of an inductively coupled plasma optical emission spectrometry (ICP-OES) using a spectrometer INTEGRA XL 2 (GBC, Dandenong Australia), equipped with a concentric nebulizer and a glass cyclonic spray chamber (both Glass Expansion, Melbourne, Australia). The analysis was performed on both the originally supplied nanoparticles and the dried nano-oxide-based samples that had been subjected to a simulation of polymerization performed according to the procedure given in the text above. During the simulation, no monomers were employed in the reaction system, whereas the other reactants and polymerization conditions were followed. After performing the reaction according to the procedure listed in Table 1 with the charge of the nano-oxide of 4 g, the aqueous phase was decanted and the inorganic powder was dried at 100 °C to a constant weight and analyzed. The contents of zinc, magnesium, and sulfur were determined by means of ICP-OES and the approximate concentrations of considered inorganic compounds (oxide, sulfate, and hydroxide) were calculated from the knowledge of the molar masses of the particular presumed compounds. In addition, the morphology of inorganic nanoparticles before

and after being subjected to polymerization conditions was observed by means of scanning electron microscopy (SEM) using a LYRA 3 scanning electron microscope (Tescan, Brno, Czech Republic). The gold-sputtered samples were examined.

For the testing of latex-based coating binder materials containing inorganic nanoparticles, free-standing films were prepared by pouring and drying the self-crosslinking latexes into silicone molds. The drying of samples proceeded first at RT ( $23 \pm 1$  °C) for a month and then at 30 °C for 2 weeks in a vacuum dryer. The wet thickness of the free-standing films was approximately 1 mm. The resulting polymer materials were investigated focusing on content and distribution of nanoparticles inside the film. The distribution of inorganic nanoparticles inside the polymer matrix was evaluated using SEM. The cryo-fractures of polymer films were examined. The concentration of embedded inorganic nanoparticles in the dried polymer material was determined by means of ICP-OES using the simplified assumption that all the determined metal (Zn, Mg) in the polymer film was only in the form of the respective oxide.

The chemical structure of the prepared materials was studied using a Fourier transform infrared (FT-IR) spectroscopy on a Nicolet iS50 instrument (Thermo Fisher Scientific, Waltham, MA, USA). The infrared spectra were obtained by an attenuated total reflectance (ATR) technique on a built-in all-reflective diamond crystal in a range from 4000 to 500  $\text{cm}^{-1}$  using the resolution of 2  $\text{cm}^{-1}$  (64 scans per spectrum).  $T_g$  of dried latex polymers was investigated using differential scanning calorimetry (DSC) on a Pyris 1 DSC instrument (Perkin-Elmer, Waltham, MA, USA) under nitrogen atmosphere at a heating rate of 10 °C/min from  $-50$  °C to 120 °C.  $T_g$  was determined using the second heating run. In addition, the degree of crosslinking introduced into latex polymers was evaluated according to gel content and crosslink density. The gel content was determined by the extraction in a Soxhlet extractor with tetrahydrofuran (THF) for 24 h according to CSN EN ISO 6427. The crosslink density was calculated from swelling experiments performed on dry gel polymer samples (around 0.2 g). The samples were immersed in toluene until equilibrium swelling was achieved (swelling at 30 °C for 7 days). The average molecular weight between crosslinks ( $M_c$ ) and the crosslink density (expressed as moles of crosslinks per  $\text{cm}^3$  of a polymer network) were calculated according to Equations (2)–(5), employing the theory of Flory and Rehner [45].

$$M_c = \frac{V_1 \rho_p [\phi^{1/3} - \phi/2]}{-[\ln(1 - \phi) + \phi + \chi \phi^2]} \quad (2)$$

$$\phi = \frac{W_p \rho_s}{W_p \rho_s + W_s \rho_p} \quad (3)$$

$$\chi = 0.34 + \frac{V_1}{RT} (\delta_1 - \delta_2)^2 \quad (4)$$

$$\text{Crosslink density} = \rho_p / M_c \quad (5)$$

where  $V_1$  is the molar volume of toluene ( $106.3 \text{ cm}^3/\text{mol}$ );  $\rho_p$  is the density of polymer that was calculated to be  $1.11 \text{ g/cm}^3$  for the BA/MMA/MAA (53/43.5/3.5 by weight) copolymer from 1.06, 1.18, and  $1.015 \text{ g/cm}^3$  for poly(BA), poly(MMA), and poly(MAA), respectively;  $\phi$  is the volume fraction of the gel polymer in the swollen gel;  $W_p$  and  $W_s$  are the weight fractions of the gel polymer and solvent (toluene) in the swollen gel, respectively;  $\rho_s$  is the density of solvent ( $0.8669 \text{ g/cm}^3$ );  $\chi$  is the polymer and solvent interaction parameter;  $\delta_1$  is the solubility parameter of polymer that was calculated to be  $9.16 \text{ (cal/cm}^3)^{1/2}$  for the BA/MMA/MAA (53/43.5/3.5 by weight) copolymer from 9.0, 9.3, and  $9.8 \text{ (cal/cm}^3)^{1/2}$  for poly(BA), poly(MMA), and poly(MAA), respectively [46,47]; and  $\delta_2$  is the solubility parameter of toluene,  $8.9 \text{ (cal/cm}^3)^{1/2}$ .

#### 2.4. Storage Stability Testing

The final self-crosslinking latex binders were stored at 50 °C for 60 days. Their storage stability was evaluated from the point of view of changes of the apparent viscosity, the average particle size and the zeta potential. The apparent viscosity of latexes was determined at 25 °C using a Brookfield LVDV-E Viscometer (Brookfield Engineering Laboratories, USA) at 100 rpm according to CSN ISO 2555. The average particle sizes and the zeta potential of polymer particles were measured by dynamic light scattering (DLS) on a Coulter N4 Plus instrument (Coulter Corp., UK). The DLS measurements were done at 25 °C.

#### 2.5. Preparation and Characterization of Coating Films

The self-crosslinking latexes were cast on glass panels using a blade film applicator coater. The thickness of wet coatings applied on glass substrates was 150 µm. No coalescing agents were used. The coatings were dried in a climatic test chamber CTC Memmert (Memmert GmbH + Co.KG, Schwabach, Germany) at 23 ± 0.1 °C and 50% ± 3% relative humidity for 7 days. The coatings were tested for their gloss, transparency, hardness, adhesion, impact resistance, chemical resistance, water absorption, and water whitening. The dry coating thickness was measured using a three-point instrument (BYK-Gardner, Geretsried, Germany).

The gloss of coatings was evaluated by a micro TRI-gloss µ instrument (BYK-Gardner, Germany) at a gloss-measuring geometry of 60°. Coatings applied on glass panels coated with a black matte paint (RAL 9005) were used for gloss measurements. The transparency of the coatings was evaluated by the light transmission (measuring the transmittance at the wavelength 500 nm) using a ColorQuest XE Spectrometer (Hunterlab, USA). The hardness of the coatings was assessed according to CSN EN ISO 1522 through measurements on a pendulum hardness tester “Persoz” (BYK-Gardner, Germany). The adhesion tests according to CSN ISO 2409 were also made. A cross-cut tester (Elcometer Instruments, Aalen, Germany) was used. The impact resistance was evaluated according CSN EN ISO using an Elcometer 1615 Variable Impact Tester (Elcometer Instruments, Germany). The chemical resistance was assessed according to ASTM D 4752 rubbing test with methyl ethyl ketone (MEK). All the experiments were carried out at RT.

The water absorption of coatings was tested by immersing free-standing films in distilled water at RT for the specified time (1, 2, 3, 7, 30, and 60 days). The free-standing films were prepared using silicone molds, as described above. At the end of the immersion period, the soaked film was removed from water and carefully blotted with filter paper. The water absorption,  $A$  is given by  $A = 100(w_t - w_0)/w_0$ , where  $w_0$  is the initial weight of a film specimen and  $w_t$  is the weight of a corresponding soaked film specimen. For each film sample, four specimens of the approximate dimensions 20 × 20 × 0.75 mm<sup>3</sup> were tested.

The water whitening of coatings cast on glass panels was assessed through measurements of transmittance on a ColorQuest XE Spectrometer (Hunterlab, Reston, VA, USA). The difference in transmittance at 500 nm (the wavelength near the green light that is most sensitive to the human eye) was ascertained. The dried coatings were immersed in distilled water at RT for the specified time (1 h and 1 day). The water-exposed coating area was measured immediately after removing the coating from water. The water whitening,  $W$ , is given by  $W = 100(T_0 - T_t)/T_0$ , where  $T_0$  is the initial coating transmittance before immersion in water and  $T_t$  is the coating transmittance after water exposure. For each latex sample, three coatings were tested.

### 3. Results and Discussion

#### 3.1. Properties of Latexes

The characteristic properties of all the prepared latexes, differing in the type and content of the added inorganic particles, are listed in Table 2. It was determined that with the increasing content of the particular inorganic oxide, being added as a component to the polymerization system, a growing mass of coagulum was formed and an increased pH value was determined, with the former indicating a drop in latex colloidal stability during the synthesis. This phenomenon can be attributed to hydration reaction of

the particular inorganic oxide resulting in the formation of the respective hydroxide (slightly soluble in water) and a small concentration of dissociated (dissolved)  $\text{OH}^-$  and  $\text{Zn}^{2+}$  or  $\text{Mg}^{2+}$  ions. Increased pH and ionic strength were therefore achieved resulting in agglomeration (coagulation) of the latex particles. When comparing both types of nano-oxides, the above-mentioned phenomena were shown to be more pronounced in the case of MgO, in all probability as the consequence of the pronouncedly increased water solubility of MgO and  $\text{Mg}(\text{OH})_2$ . For a better comparison, see the available data: ZnO and MgO solubility in water at an ambient temperature is ca.  $1.6 \times 10^{-4}$  and  $8.6 \times 10^{-3}$  g/100 mL, respectively. The pH of a saturated nano-oxide water slurry is about 8.6 and 10.4 for ZnO and MgO, respectively, calculated from the respective solubility data of ca.  $2.0 \times 10^{-6}$  M for  $\text{Zn}(\text{OH})_2$  and  $1.4 \times 10^{-4}$  M for  $\text{Mg}(\text{OH})_2$ . Moreover, the a strongly acidic environment of the polymerization system (caused by the presence of polyglycol ether sulfate-based emulsifier and especially by the presence of the ammonium persulfate initiator producing sulfuric acid as the result of the reaction with water) probably induced another significant dissolution of the particular nano-oxide during the polymerization process leading to the formation of highly soluble in water sulfates (zinc or magnesium) and also to the enhanced solubility of the nascent hydroxides ( $\text{Zn}(\text{OH})_2$  or  $\text{Mg}(\text{OH})_2$ ) in water.

**Table 2.** Characteristics of self-crosslinking latex binders differing in type and content of inorganic nanoparticles.

Sample	Charge of Nanoparticles (wt %) <sup>1</sup>	Coagulum Content (wt %) <sup>2</sup>	pH <sup>2</sup>	MFFT (°C) <sup>3</sup>
L <sub>0</sub>	0	0.4 ± 0.08	2.21 ± 0.04	8.2 ± 0.25
L <sub>ZnO-0.5</sub>	0.5	0.5 ± 0.12	5.70 ± 0.09	10.4 ± 0.12
L <sub>ZnO-1.0</sub>	1.0	0.6 ± 0.16	6.03 ± 0.06	11.2 ± 0.20
L <sub>ZnO-1.5</sub>	1.5	0.8 ± 0.21	6.11 ± 0.08	12.6 ± 0.26
L <sub>ZnO-2.0</sub>	2.0	1.1 ± 0.27	6.24 ± 0.11	13.8 ± 0.21
L <sub>MgO-0.5</sub>	0.5	1.0 ± 0.32	7.20 ± 0.12	4.7 ± 0.31
L <sub>MgO-1.0</sub>	1.0	2.4 ± 0.21	8.38 ± 0.23	2.8 ± 0.14
L <sub>MgO-1.5</sub>	1.5	5.0 ± 0.59	10.19 ± 0.25	2.0 ± 0.26
L <sub>MgO-2.0</sub>	2.0	9.1 ± 0.72	10.29 ± 0.15	1.5 ± 0.14

<sup>1</sup> Based on total monomer feeds. <sup>2</sup> Determined before ammonia and ADH addition to the latex. <sup>3</sup> Determined after ammonia and ADH addition to the latex.

In addition, the impact of nanoparticle type and content on MFFT of the resulting self-crosslinking latexes (i.e., latexes after eventual ammonia alkalization and ADH addition) was studied. In the case of latexes containing ZnO nanoparticles, an increase in MFFT values was observed with the increasing content of added nanoparticles. As the latexes contained dissociated  $\text{Zn}^{2+}$  ions, ionic interfacial self-crosslinking via carboxylic acid functional groups of emulsion polymer was probably proceeding during film-formation. The particle flattening and inter-diffusion of polymer chains were therefore deteriorated during the coalescence stage, resulting in MFFT enhancement. In contrast, MFFT decrease was observed with the increasing content of MgO nanoparticles. In this case, the existence of ionic crosslinking cannot be denied, but the pronounced fall of MFFT is apparently related especially to hydroplasticization of carboxylated polymer, which occurred due to the permanent neutralization of a great extent of carboxylic functionalities (in comparison with the reference latex L<sub>0</sub> and the ZnO-based latexes that comprise protonated carboxylic groups after ammonia evaporation). As all the MgO-based latexes were alkaline (see Table 2) due to a considerable amount of dissolved  $\text{Mg}(\text{OH})_2$  in water, the plasticization of latex polymer by water was apparently achieved during the entire process of film drying via the existence of ionized carboxylic groups. This resulted in a decrease in MFFT.

### 3.2. Inherent Structure of Coating Binders

As the nano-sized inorganic oxides were supposed to be chemically transformed in the course of latex synthesis, a simulation of the effect of the polymerization conditions and reactants on the character

of the nanoparticles was performed without employing the monomers in the reaction system for better analysis accuracy. The original and the resulting chemical nature of the inorganic nanoparticles, originating from the respective metal oxide, were investigated by means of the XRD spectroscopy. It was determined (see Figure 1) that the original chemical nature of the nano-sized ZnO exhibited a structure of zincite (amorphous ZnO) which changed to zinc sulfate hydroxide ( $\text{ZnSO}_4 \cdot 3\text{Zn}(\text{OH})_2$ ) to a great extent, after being subjected to polymerization conditions. The chemical conversion of ZnO nanoparticles in the strongly acidic aqueous environment of the polymerization system is represented by Reaction (6) [48]. The MgO nanoparticles, formed in their original state by both periclase ( $\text{MgO}$ ) and brucite ( $\text{Mg}(\text{OH})_2$ ), were shown to be converted almost entirely into  $\text{Mg}(\text{OH})_2$ . The conversion of MgO into  $\text{Mg}(\text{OH})_2$  is represented by Reaction (7).

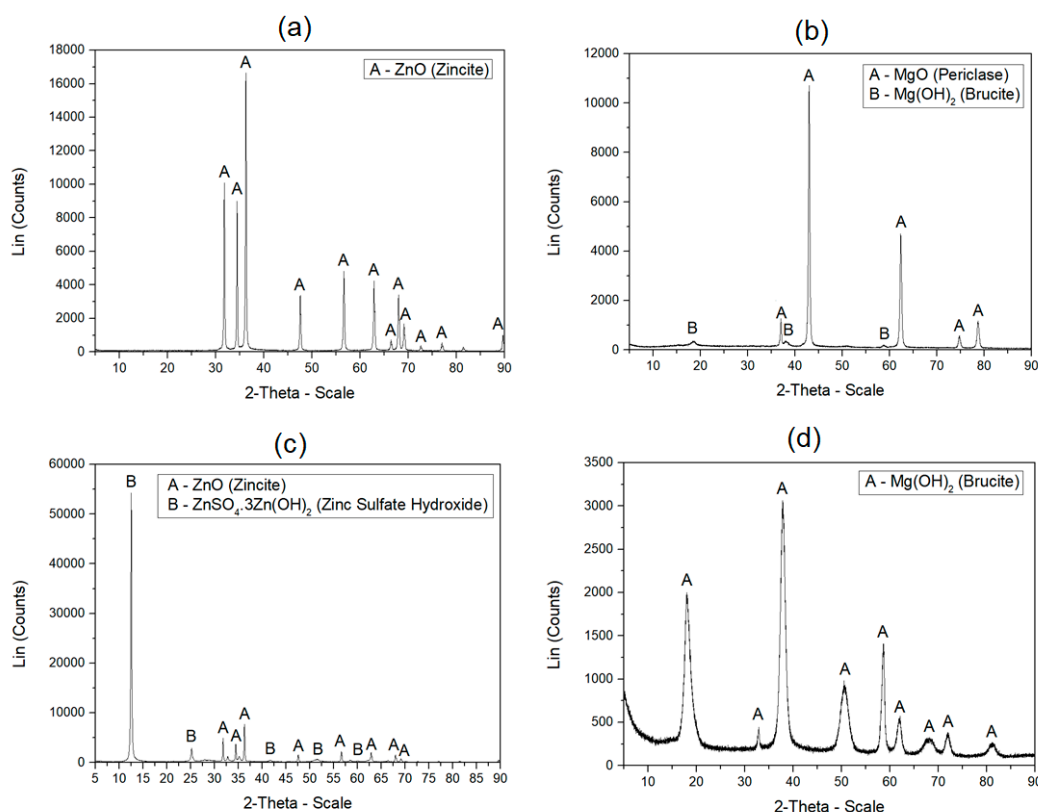


**Figure 1.** XRD patterns of inorganic nanoparticles: (a) originally supplied ZnO; (b) originally supplied MgO; (c) ZnO affected by polymerization conditions; (d) MgO affected by polymerization conditions.

In addition, the inorganic nanoparticles in the original state and after being subjected to polymerization conditions were tested using ICP-OES. Similarly to XRD results, it was determined (see Tables 3 and 4) that the oxide-based original character changed largely to hydroxide and sulfate in the case of nano-sized ZnO, whereas the MgO nanoparticles turned almost completely into  $\text{Mg}(\text{OH})_2$ . It should be mentioned here, however, that before the XRD and ICP-OES analyses, the nanoparticles (subjected to the polymerization-like treatment) had been isolated from the aqueous environment by decantation followed by air-drying. Therefore, apparently a significant amount of dissolved sulfates ( $\text{ZnSO}_4$  or  $\text{MgSO}_4$ ) had been removed and the analyzed samples did not in all probability fully correspond to reality (in terms of the corresponding latex coating samples).

**Table 3.** ICP-OES results of inorganic nanoparticles before and after being subjected to polymerization conditions.

Nanoparticle Type	Original State				Final State			
	Zn (g/kg)	Mg (g/kg)	S (g/kg)	Remainder (g/kg) <sup>1</sup>	Zn (g/kg)	Mg (g/kg)	S (g/kg)	Remainder (g/kg) <sup>1</sup>
ZnO	798.0 ± 0.11	0	0.07 ± 0.05	291.93 ± 0.11	655.0 ± 0.11	0	41.10 ± 0.105	303.90 ± 0.11
MgO	0	570.0 ± 0.09	0.15 ± 0.07	429.85 ± 0.09	0	406.0 ± 0.11	8.68 ± 0.05	585.32 ± 0.11

<sup>1</sup> The remainder is assumed to be represented mostly by O and H.

**Table 4.** Estimation of nanoparticle character before and after being subjected to polymerization conditions. Results were calculated using ICP-OES results and molar masses of presumed compounds.

Nanoparticle Type	Original State			Final State		
	Oxide (wt %)	Hydroxide (wt %)	Sulfate (wt %)	Oxide (wt %)	Hydroxide (wt %)	Sulfate (wt %)
ZnO	96.4	3.6	~0	34.0	45.3	20.7
MgO	82.6	17.3	~0	~0	96.7	3.3

To illustrate the effect of polymerization conditions on the microstructure of inorganic particles, the particle morphology before and after polymerization-like treatment was compared using SEM, as shown in Figure 2. It can be seen clearly that both nano-oxides in their original state were formed by agglomerates made of distinct nanoparticles in the size of tens to hundreds of nanometers. After being subjected to the acidic aqueous environment, a slight increase in particle size was observed in the case of ZnO, which may be assigned to hydration of the nanoparticle surface resulting in covering by a layer of  $\text{ZnSO}_4 \cdot 3\text{Zn}(\text{OH})_2$ . In the case of MgO, the original agglomerates made of spherical nanoparticles changed to lamellar-like structures, which is a typical particle morphology for nanostructured  $\text{Mg}(\text{OH})_2$  [49].

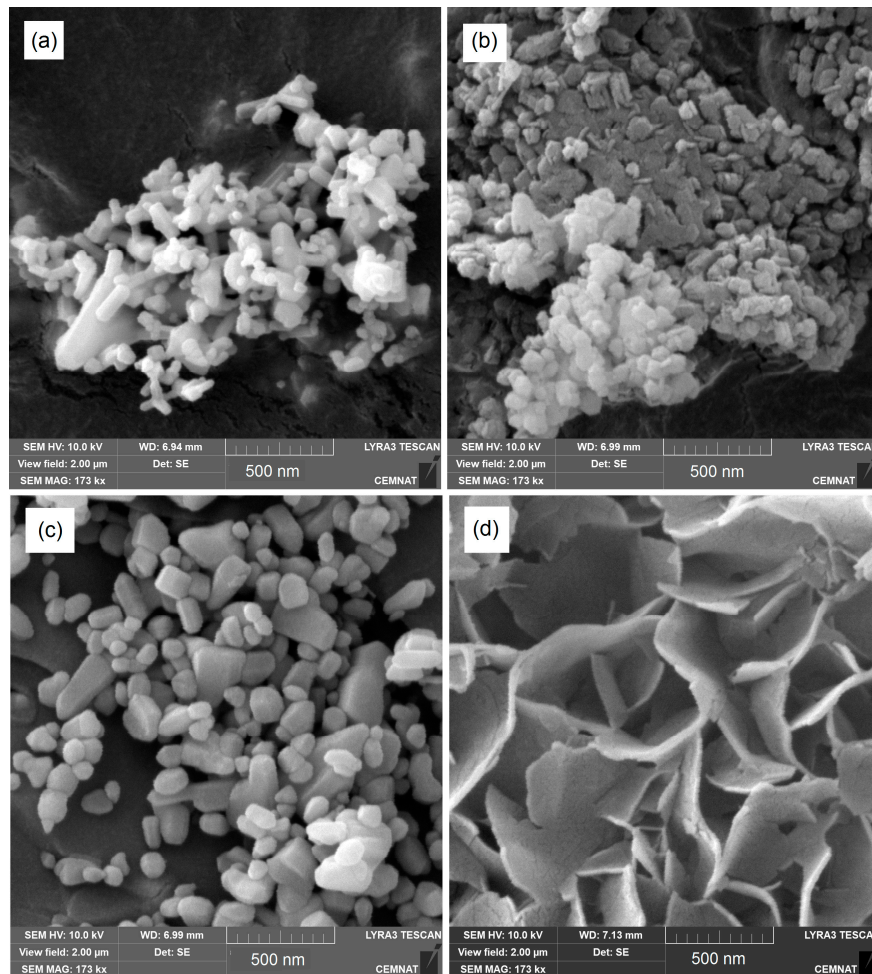


**Figure 2.** SEM photographs of inorganic nanoparticles: (a) originally supplied ZnO; (b) originally supplied MgO; (c) ZnO affected by polymerization conditions; (d) MgO affected by polymerization conditions.

In addition, the morphology and distribution of inorganic nanoparticles incorporated into latexes during emulsion polymerization was investigated on dried coating film materials. Figure 3 illustrates the cryo-fracture surfaces of a neat latex polymer (sample  $L_0$ ), a ZnO-based polymer material (sample  $L_{\text{ZnO-2.0}}$ ) and a corresponding MgO-based polymer material (sample  $L_{\text{MgO-2.0}}$ ). SEM micrographs were taken in both secondary electron (SE) mode (demonstrating the topographic view) and backscattered electron (BSE) mode (representing the elementary contrast of the surface). It is evident that the dried polymer materials contained no micro-sized inorganic agglomerates. The inorganic additives were in the form of primary nanoparticles that were deployed regularly inside the polymer matrix, which is a favorable condition for the transparent nature of the final coatings. When comparing both types of inorganic nano-oxides, ZnO-based nanoparticles occurred in the form

of spheres, whereas MgO-based nanoparticles exhibited a lamellar morphology, which correlates well with the SEM observations presented in Figure 2.

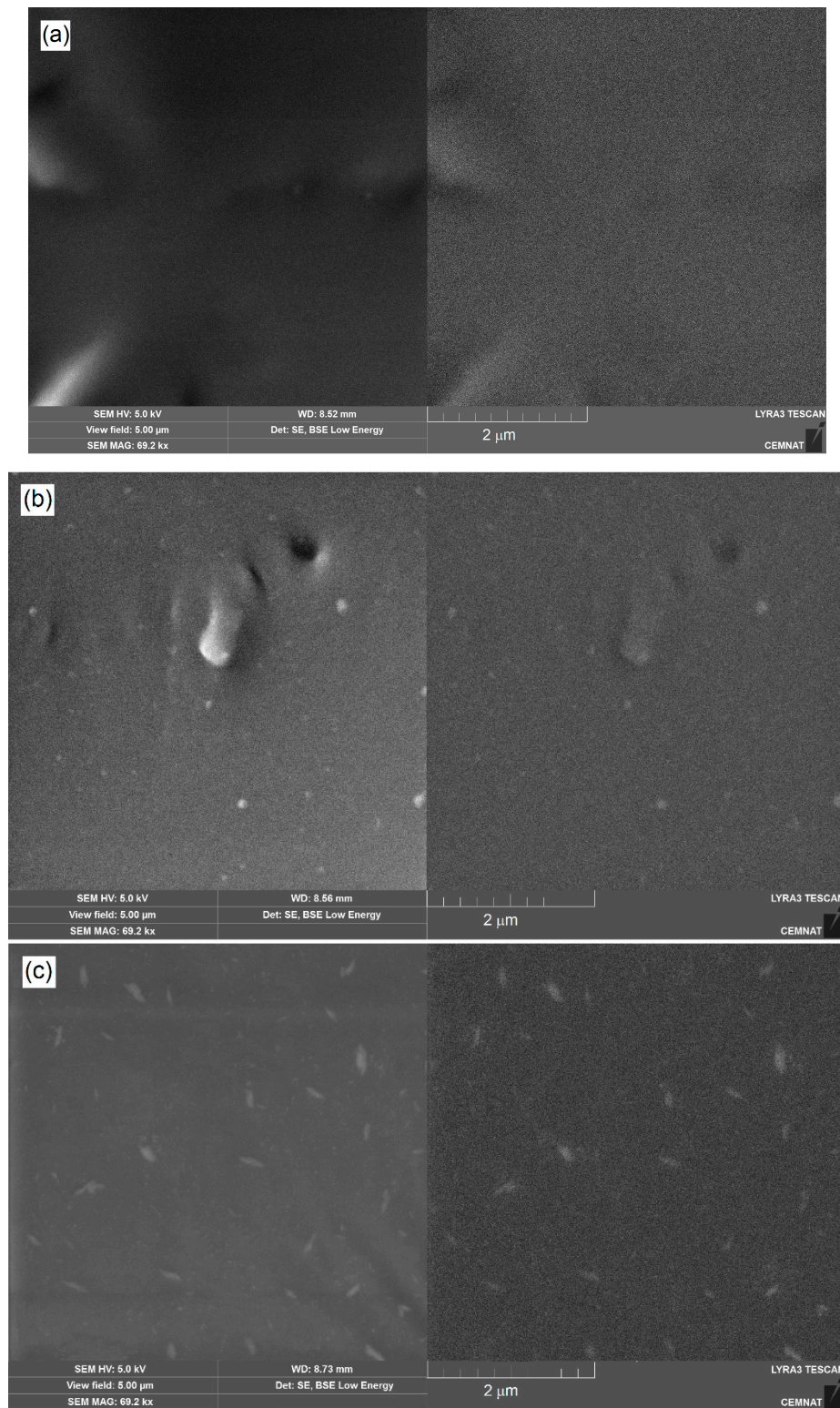


**Figure 3.** SEM images of cryo-fractures of coating samples taken in SE mode (left) and BSE mode (right): (a) sample  $L_0$  without nanoparticles; (b) sample  $L_{ZnO-2.0}$  containing ZnO-based nanoparticles; (c) sample  $L_{MgO-2.0}$  containing MgO-based nanoparticles.

The content of inorganic nanoparticles, embedded into the polymer coating matrix, was also investigated. As the latexes contained a significant content of coagulum (see Table 2), the actual concentration of nanoparticles in the coatings was assumed to be lower than the corresponding theoretical concentration. The ICP-OES measurements (see Table 4) confirmed this expectation, finding that with the increasing charge of both types of nano-oxides, the portion of the nanoparticles, being dissolved or stably dispersed in the aqueous latex medium in the form of various metal compounds (we especially consider the forms of oxide, hydroxide, and sulfate), decreased, whereas the proportion of nanoparticles trapped in the form of coagulum increased. Therefore, efforts to further increase the nanoparticle content in the resulting coating material (by means of the nano-oxide addition in the course of latex synthesis procedure), seem to be inefficient.

The chemical structure of the prepared emulsion polymers containing inorganic nanoparticles was analyzed using FT-IR spectroscopy. Absorption spectra of the representative latex materials  $L_0$ ,  $L_{ZnO-2.0}$ , and  $L_{MgO-2.0}$  differing in nanoparticle presence and type are presented in Figure 4. It can be seen that the spectra display a typical pattern of acrylic polymers with a characteristic strong absorption band of C=O bond at  $1735\text{ cm}^{-1}$  assigned to carboxylic acid ester group. The absorption bands at  $2961\text{ cm}^{-1}$  and  $2873\text{ cm}^{-1}$  can be attributed to asymmetric  $\nu_a(\text{C-H})$  and symmetric  $\nu_s(\text{C-H})$  vibrations of  $\text{CH}_3$  group. The weak absorption band of  $\nu_a(\text{C-H})$  and a shoulder of  $\nu_s(\text{C-H})$ , which appeared at  $2934\text{ cm}^{-1}$  and  $2853\text{ cm}^{-1}$ , respectively, were related to vibrations of the  $\text{CH}_2$  group. The characteristic absorption band at  $1537\text{ cm}^{-1}$  appearing in all the spectra was assigned to bending vibration of N-H bonds and proves that DAAM was copolymerized with acrylic monomers. All the polymers further manifested a weak absorption band at  $1652\text{ cm}^{-1}$  corresponding in all probability to N=C vibration, which indicates that the keto-hydrazide self-crosslinking reaction proceeded in latex polymers [50]. In addition, a broad absorption band of O-H bond at  $3440\text{--}3250\text{ cm}^{-1}$  appeared in all the latex samples, being the most significant in the case of  $L_{MgO-2.0}$ . This absorption band was assigned to the protonated carboxylic group (from MAA), hydrogen bonded water and inorganic hydroxides (in case of samples with embedded nanoparticles). The highest intensity of this band in the case of MgO incorporation may be attributed to enhanced solubility of MgO in water (in contrast to ZnO) leading to dissolved  $\text{Mg}(\text{OH})_2$ , which caused a higher degree of ionization (neutralization) of the carboxylic groups. The neutralized carboxylic groups were responsible for imparting a higher amount of molecularly bonded (hydroplasticizing) water in latex copolymers [51,52]. Moreover, a weak absorption band corresponding to carboxylate anion  $\nu_a(\text{COO})$  appeared at  $1600\text{ cm}^{-1}$  in the spectra of samples  $L_{ZnO-2.0}$  and  $L_{MgO-2.0}$ , which proves again the presence of carboxylic acid salts and also suggests the existence of ionic self-crosslinking between carboxylic groups and dissociated bivalent metal cations. Similarly, this band was shown to be more pronounced in the case of the MgO-based sample, which again reveals a higher extent of carboxylic group ionization.

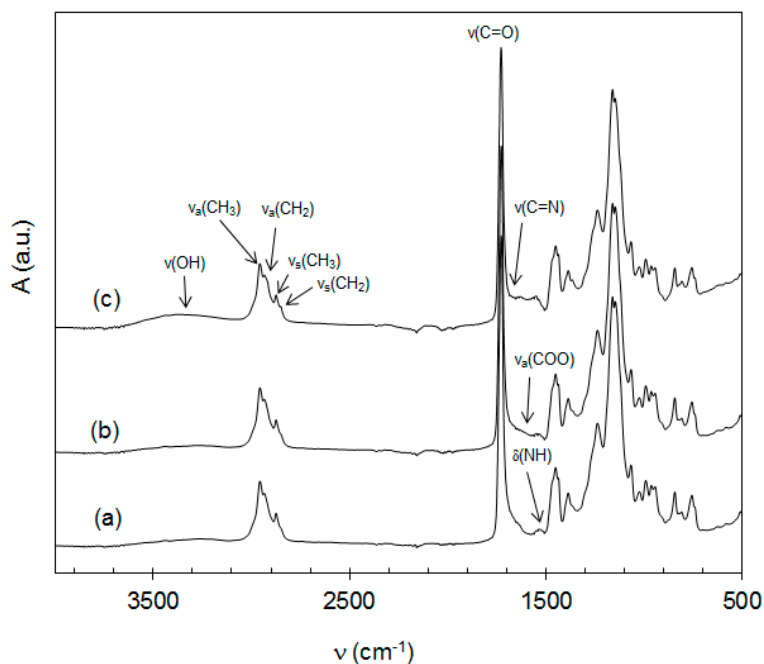


**Figure 4.** FT-IR spectra of latex materials: (a) sample  $L_0$  without nanoparticles; (b) sample  $L_{ZnO-2.0}$  containing ZnO-originated nanoparticles; (c) sample  $L_{MgO-2.0}$  containing MgO-originated nanoparticles.

The effect of nanoparticle type and content on the structure of latex-based coating binder materials was also studied from the point of view of  $T_g$ . Table 5 demonstrates that in the case of nano-sized ZnO incorporation, a decrease in  $T_g$  can be observed at lower contents of nanoparticles (samples  $L_{ZnO-0.5}$  and  $L_{ZnO-1.0}$ ) followed by a slight  $T_g$  elevation at higher concentrations of embedded nanoparticles (samples  $L_{ZnO-1.5}$  and  $L_{ZnO-2.0}$ ). This phenomenon may be ascribed to the competing effects of hydroplasticization (decreasing  $T_g$ ) and ionic self-crosslinking (increasing  $T_g$ ), both being influenced by dissolved zinc hydroxide molecules. The latex polymers containing MgO-based nanoparticles were shown to exhibit a marked decrease in  $T_g$ , being more pronounced with the increased content of nanoparticles. As discussed above, this effect suggests a significant hydroplasticization of carboxylated polymer caused by the high solubility of  $Mg(OH)_2$  in the aqueous dispersion medium (in comparison with zinc hydroxide in ZnO-based latexes) providing a great extent of neutralization of carboxylic functional groups in emulsion polymer. The DSC measurements also revealed that the polymers containing the MgO-based nanoparticles (except for the sample  $L_{MgO-0.5}$  with the lowest nanoparticles content) exhibited a pronounced second relaxation phenomenon at a temperature in a range of 61–68 °C (see the demonstrative DSC record in Figure 5). This phenomenon is probably related to the existence of ionic clusters formed by associated ionized carboxylic functionalities and metal cations, acting as interfacial crosslinking knots. The ionic clusters are believed to form a separate phase which can be manifested as a second glass transition in the DSC curve or eventually as a second maximum in the temperature dependence of loss factor, appearing at a higher temperature than that corresponding to the main polymer [14,53,54]. As the ionic bonds are temperature sensitive, they had obviously been destroyed during the first heating cycle and thus did not already occur in the second heating curve.

**Table 5.** Effect of type and content of inorganic nanoparticles on  $T_g$ , gel content,  $M_c$  and crosslink density of coating binder materials.

Sample	Theoretical Content of Nanoparticles (wt %) <sup>1</sup>	Metal Content (mg/kg)	Real Content of Nanoparticles (wt %) <sup>2</sup>	$T_g$ (°C)	Gel Content (wt %)	$M_c$ (g/mol)	Crosslink Density (moles/cm <sup>3</sup> )
L <sub>0</sub>	0	0	0	15.0 ± 0.24	75.0 ± 2.2	111,365 ± 3849	1.00 × 10 <sup>-5</sup>
LZnO-0.5	0.5	3752 ± 31	0.47 ± 0.003	13.6 ± 0.28	88.8 ± 1.9	27,462 ± 2750	4.04 × 10 <sup>-5</sup>
LZnO-1.0	1.0	6120 ± 65	0.76 ± 0.008	13.3 ± 0.16	90.6 ± 1.2	24,308 ± 1452	4.57 × 10 <sup>-5</sup>
LZnO-1.5	1.5	7122 ± 49	0.89 ± 0.005	13.9 ± 0.31	91.1 ± 2.3	23,231 ± 31098	4.78 × 10 <sup>-5</sup>
LZnO-2.0	2.0	8741 ± 75	1.09 ± 0.009	14.2 ± 0.27	92.2 ± 0.9	22,104 ± 1220	5.02 × 10 <sup>-5</sup>
LMgO-0.5	0.5	2851 ± 25	0.47 ± 0.004	11.7 ± 0.45	90.1 ± 1.8	16,508 ± 954	6.79 × 10 <sup>-5</sup>
LMgO-1.0	1.0	4931 ± 30	0.82 ± 0.005	8.3 ± 0.32 <sup>3</sup>	92.9 ± 2.4	9893 ± 556	1.13 × 10 <sup>-4</sup>
LMgO-1.5	1.5	6339 ± 42	1.07 ± 0.007	5.6 ± 0.61 <sup>3</sup>	94.7 ± 1.6	9620 ± 249	1.16 × 10 <sup>-4</sup>
LMgO-2.0	2.0	6574 ± 90	1.09 ± 0.015	4.0 ± 0.47 <sup>3</sup>	95.6 ± 1.9	9220 ± 276	1.21 × 10 <sup>-4</sup>

<sup>1</sup> Percentage of inorganic nanoparticles with respect to polymer mass. <sup>2</sup> Percentage of inorganic nanoparticles in a dried polymer film calculated from ICP-OES results using the simplified assumption that all the determined metal (Zn, Mg) in the polymer film was only in the form of the respective oxide. <sup>3</sup> The sample also exhibited a second glass transition appearing in the first heating curve in a temperature range of 61–68 °C.

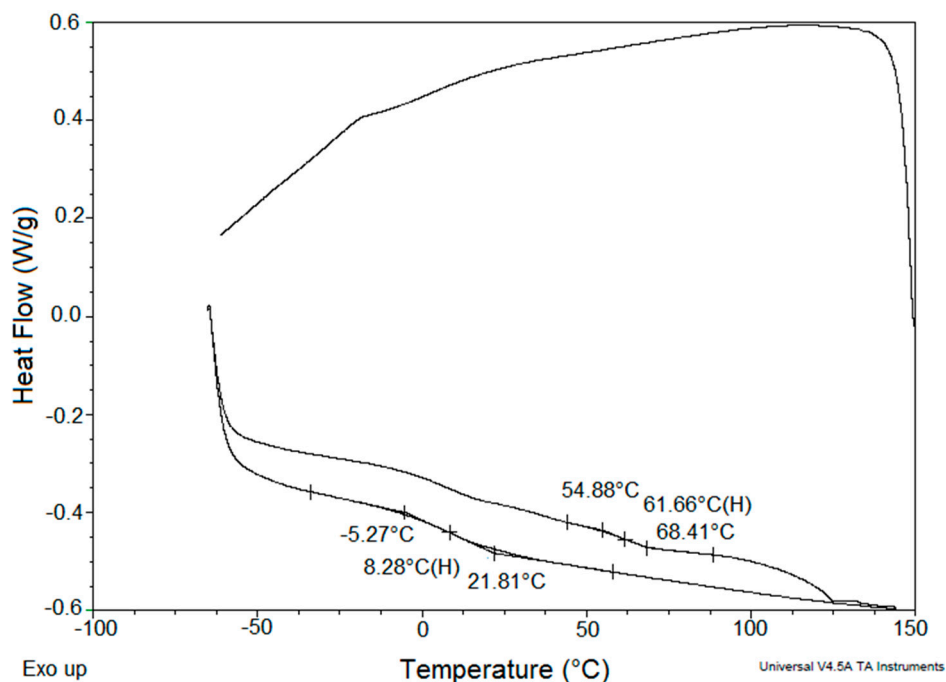


**Figure 5.** DSC record for the sample  $L_{MgO-1.0}$  containing MgO-based nanoparticles. Illustration of a second iso-phase transition appearing in the first heating curve.

The level of chemical (covalent) and physical (ionic) crosslinking introduced into emulsion polymers by means of keto-hydrazide reaction and bivalent metal ions originated from the nano-sized oxides, respectively, was evaluated from according to results of gel content and crosslink density (see Table 5). It was determined that the gel content and crosslink density increased with the growing content of embedded inorganic nanoparticles, which proves the formation of physical ionic crosslinks. When comparing both types of nano-oxides in the role of ionic self-crosslinking agents, MgO was found to be more effective. The reason is probably related to its higher solubility providing a higher concentration of dissociated metal ions and a higher amount of neutralized carboxylic groups, as has been already discussed above. Moreover, we believe that due to plasticization of emulsion polymers, carboxylic groups—both on the particle surface and buried in the particle interior—were involved, providing ionic inter- and intra-particle crosslinks. At this stage, it should be mentioned that the ionic intra-particle crosslinking is thought to have proceeded already during the polymer synthesis after dosing the nanostructured MgO into the reactor.

### 3.3. Storage Stability of Self-Crosslinking Latexes

The occurrence of increased coagulum content formed during latex synthesis and the possibility of premature ionic inter-particle crosslinking indicated a danger of reduced colloidal stability of the self-crosslinking one-component latexes containing the inorganic nanoparticles. Therefore, the storage stability of latexes was also tested from the point of view of changes of the apparent viscosity, the average particle size and the zeta potential before and after long-term storing of latexes at the elevated temperature. It was shown (see Table 6) that the initial values of the particle size and viscosity were not significantly affected by the addition of nano-oxides in the case of samples containing ZnO-based nanoparticles. On the contrary, the alkali-swelling effect [55], demonstrated by the increase in particle size and viscosity, was observed in the case of MgO-based latex samples, appearing more distinctly with the increasing content of added nanoparticles. It was also found that the initial zeta potential values decreased with the growing amount of incorporated nano-oxides. This was more pronounced in the case of MgO and can be attributed to enhanced ionic strength due to dissolution of the particular metal oxide. For the series of latexes containing MgO-based nanoparticles, zeta

potential values close to  $-30$  mV revealed the risk of incipient instability and additionally certified a pronounced coagulum formation during the synthesis of these latexes (see Table 2). Despite our doubts, no significant changes of the tested properties were found after storing. All latex samples (including the latexes of the MgO-based series) were shown to resist aggregation—i.e., no sedimentation—sagging, and no apparent coagulum was formed during storing at the elevated temperature. In view of this fact, all the prepared latex coating binders can be considered sufficiently stable in the long term.

**Table 6.** Results of storage stability testing (in terms of particle size, zeta potential, and viscosity) of self-crosslinking latex binders differing in type and content of inorganic nanoparticles before and after storing at  $50$  °C for 60 days.

Sample	Same Day of Synthesis			After Storage		
	Particle Size (nm)	Zeta Potential (mV)	Viscosity (mPa.s)	Particle Size (nm)	Zeta Potential (mV)	Viscosity (mPa.s)
L <sub>0</sub>	103.4 ± 0.4	−39.5 ± 1.0	19.3 ± 0.15	104.7 ± 0.7	−42.7 ± 1.3	20.8 ± 0.14
L <sub>ZnO-0.5</sub>	98.4 ± 0.9	−38.2 ± 0.5	25.4 ± 0.43	98.8 ± 1.4	−40.4 ± 2.7	21.6 ± 0.56
L <sub>ZnO-1.0</sub>	92.9 ± 0.6	−35.6 ± 1.2	31.9 ± 0.28	94.0 ± 0.8	−38.9 ± 0.9	27.5 ± 0.20
L <sub>ZnO-1.5</sub>	87.7 ± 0.8	−34.0 ± 1.1	24.2 ± 0.36	88.3 ± 0.9	−36.7 ± 2.6	31.3 ± 0.34
L <sub>ZnO-2.0</sub>	98.8 ± 1.1	−33.5 ± 0.9	28.7 ± 0.11	99.5 ± 1.2	−39.5 ± 2.1	33.5 ± 0.08
L <sub>MgO-0.5</sub>	121.3 ± 0.7	−32.2 ± 0.8	21.2 ± 0.33	122.9 ± 1.1	−30.5 ± 0.5	23.2 ± 0.38
L <sub>MgO-1.0</sub>	150.3 ± 1.2	−31.0 ± 0.5	31.3 ± 0.22	156.3 ± 0.9	−27.8 ± 0.6	34.3 ± 0.32
L <sub>MgO-1.5</sub>	155.7 ± 1.3	−29.4 ± 1.0	38.9 ± 0.26	163.5 ± 1.2	−28.1 ± 0.8	40.0 ± 0.29
L <sub>MgO-2.0</sub>	161.1 ± 1.4	−29.0 ± 1.1	44.2 ± 0.43	167.6 ± 1.5	−26.9 ± 0.7	46.1 ± 0.37

### 3.4. Coating Properties

The effects of type and content of added inorganic nano-oxides on the coating properties are presented in Table 7. The thickness of the dried coatings was approximately  $60$   $\mu\text{m}$ . All the coatings were found to be smooth and highly transparent, as shown in Figure 6. All the prepared coatings exhibited a high gloss regardless the type and content of the nanoparticles. The high gloss of the latex films suggests the nano-sized nature of the inorganic particles and well-coalesced of coating films. In addition, the physico-mechanical properties of the coatings were evaluated. When comparing film hardness regarding the added nano-oxide type, the results revealed that the presence of ZnO-based nanoparticles had no significant effect on the initial and final hardness of coatings, whereas the presence of embedded MgO-based nanoparticles caused a decrease in film hardness, which can be attributed to hydroplasticization of latex polymer, as discussed in more detail above. It was also found that the embedded nanoparticles did not deteriorate film adhesion and impact resistance and provided excellent MEK resistance of coating films, which was in all probability caused by the combination of covalent and ionic self-crosslinking, providing increased crosslink density of polymer coating films.



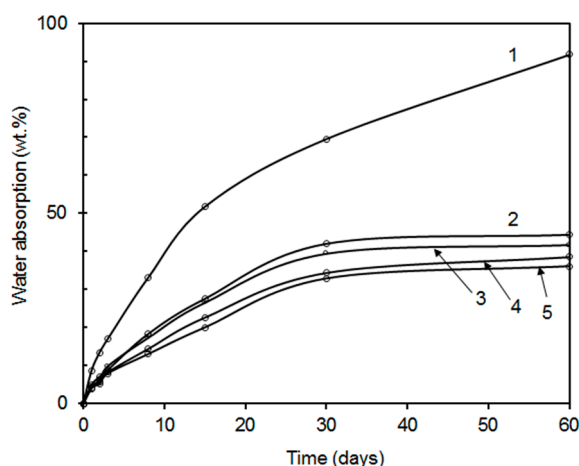
**Figure 6.** Appearance of coatings cast on glass substrates.

Table 7. Properties of coatings cast on glass substrates.

Sample	Thickness ( $\mu\text{m}$ )	Transmittance (%) <sup>1</sup>	Gloss 60° (GU)	Initial Hardness (%) <sup>2</sup>	Final Hardness (%) <sup>3</sup>	Adhesion (Degree of Flaking)	Impact Resistance (cm)	MEK Resistance (Number of Strikes)
L <sub>0</sub>	61.5 ± 5.8	90.8 ± 0.26	82.4 ± 0.4	28.7 ± 0.6	33.5 ± 0.7	0 <sup>4</sup>	above 100 <sup>4</sup>	28 ± 1.5
L <sub>ZnO-0.5</sub>	58.1 ± 8.3	90.6 ± 0.33	83.8 ± 0.9	27.4 ± 0.4	29.6 ± 0.7	0	above 100	200 ± 2.
L <sub>ZnO-1.0</sub>	55.2 ± 6.7	90.3 ± 0.17	82.9 ± 0.5	27.7 ± 0.5	30.0 ± 1.0	0	above 100	above 300 <sup>4</sup>
L <sub>ZnO-1.5</sub>	53.5 ± 7.1	90.7 ± 0.34	81.2 ± 0.6	28.9 ± 0.4	31.2 ± 0.5	0	above 100	above 300
L <sub>ZnO-2.0</sub>	58.8 ± 8.6	91.0 ± 0.22	83.7 ± 0.3	30.4 ± 0.6	33.2 ± 0.8	0	above 100	above 300
L <sub>MgO-0.5</sub>	60.2 ± 7.4	90.9 ± 0.44	83.0 ± 0.3	18.7 ± 0.8	22.9 ± 1.1	0	above 100	215 ± 3
L <sub>MgO-1.0</sub>	60.5 ± 6.3	91.0 ± 0.36	82.4 ± 1.1	13.7 ± 0.7	15.0 ± 0.7	0	above 100	above 300
L <sub>MgO-1.5</sub>	57.7 ± 8.0	90.7 ± 0.17	81.7 ± 0.4	12.2 ± 0.4	14.1 ± 0.5	0	above 100	above 300
L <sub>MgO-2.0</sub>	48.3 ± 5.0	90.6 ± 0.34	82.6 ± 1.0	11.0 ± 0.2	13.2 ± 0.3	0	above 100	above 300

<sup>1</sup> Transmittance measured at 500 nm. <sup>2</sup> Hardness after drying for 1 day. <sup>3</sup> Hardness after drying for 7 days. <sup>4</sup> Maximum evaluative value (representing the best property).

It is known that a serious disadvantage of latex coatings is a poor water resistance, usually accompanied with water whitening, loss of adhesion, and deterioration of mechanical properties. As increasing crosslink density has been used as an effective way to enhance water resistivity of latex coatings [13,56], the prepared coating films combining covalent and ionic self-crosslinking were also subjected to testing of water resistance (symbolized by water absorption and water whitening). The time curves of water absorption into coating films are displayed in Figures 7 and 8. Similar water absorption trends can be observed for both series of coatings differing in the nano-oxide type, the higher the content of inorganic nanoparticles, the lower the water absorption. This effect correlates well with the results of crosslink density summarized in Table 5. When comparing both types of inorganic crosslinkers, the MgO-based coatings exhibited higher water resistance in terms of the values of water absorption at later stages of water exposure, which corresponds to the higher crosslink density and stiffness of latex polymer, restricting both the diffusion of water and growing of water domains within the latex film. In contrast, nanostructured MgO provided coatings with a higher water uptake at early stages of exposure in water, which can be associated with a higher concentration of dissolved ionic inorganic compounds trapped in interstices between coalesced latex particles, giving rise to osmotic pressure increase (as the main driving force of water absorption) and enhanced water absorption at early stages of water exposure. After the extraction of these hydrophilic components by water, the osmotic pressure was reduced, which even resulted in a drop in water uptake in case of films with higher contents of added MgO (coating samples  $L_{ZnO-1.0}$ ,  $L_{ZnO-1.5}$ , and  $L_{ZnO-2.0}$ ).



**Figure 7.** Water absorption into coating films prepared from the latexes containing ZnO-based nanoparticles: sample  $L_0$  without nanoparticles (curve 1); sample  $L_{ZnO-0.5}$  (curve 2); sample  $L_{ZnO-1.0}$  (curve 3); sample  $L_{ZnO-1.5}$  (curve 4); sample  $L_{ZnO-2.0}$  (curve 5). The standard deviations of performed measurements were below 2%.

Additionally, water whitening of coatings was monitored by means of changes in transmittance (see Figure 9). It is known that water whitening of a coating film is in a close relationship with the polymer network density, as the number and size of water domains, scattering light of longer wavelengths, are limited by the rigidity of the polymer [52]. Therefore, coating films exhibiting marked water absorption usually suffer from pronounced water whitening [57]. As expected, the water whitening results were in a good agreement with the results of water absorption, i.e., a water whitening tendency was reduced with the increasing level of ionic self-crosslinking. At this stage, it should be emphasized that latexes synthesized using higher contents of MgO (1, 1.5, and 2 wt % with respect to total monomer feeds) were found to provide considerably water whitening resistant coatings, which can be ascribed to imparting a high level of ionic crosslinking in the resulting latex film.

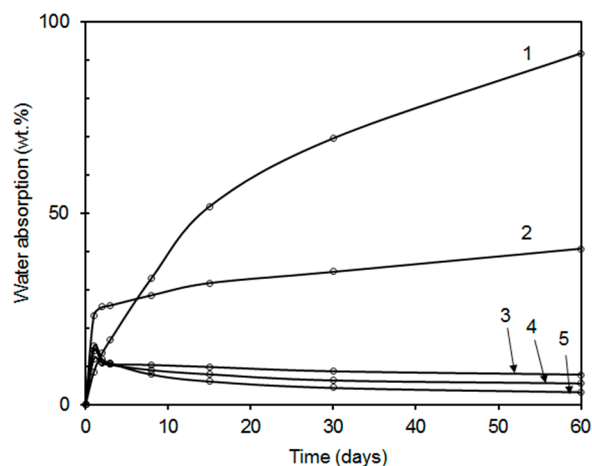


**Figure 8.** Water absorption into coatings prepared from the latexes containing MgO-based nanoparticles: sample L<sub>0</sub> without nanoparticles (curve 1); sample L<sub>MgO-0.5</sub> (curve 2); sample L<sub>MgO-1.0</sub> (curve 3); sample L<sub>MgO-1.5</sub> (curve 4); sample L<sub>MgO-2.0</sub> (curve 5). The standard deviations of performed measurements were below 2%.

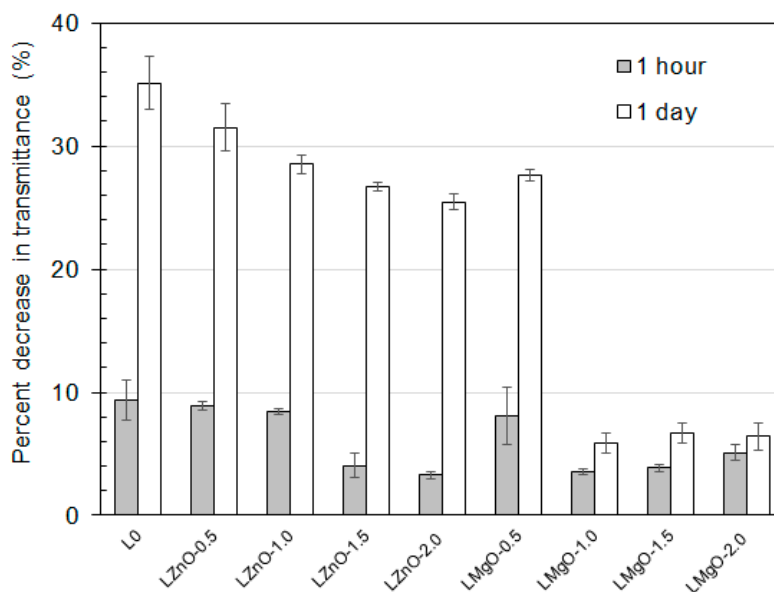


**Figure 9.** Water whitening (symbolized by transmittance decrease) of coatings applied on glass panels after their exposure in water for 1 h (grey columns) and 1 day (white columns).

#### 4. Conclusions

The present work was devoted to high-performance latex coating binders using nanostructured ZnO and MgO as functional additives. To overcome the typical shortcomings of latex coatings, the interfacial self-crosslinking was introduced into polymer films by the combination of the covalent keto-hydrazide reaction and ionic bonding due to bivalent metal ions originating from the nano-sized oxides. It was demonstrated that the powdered nano-oxides without any surface treatment could be successfully incorporated into the latex already during the process of emulsion polymerization. In this way, long-term stable latexes comprising dispersed inorganic nanoparticles (in the content of ca 0.5–1.1 wt % with respect to total solids) were prepared easily, although increased mass of coagulum was formed during polymerization at higher amounts of MgO incorporation. Both types of inorganic nano-oxides were found to act as effective ionic crosslinkers providing superior MEK resistance of coatings without deteriorating coating gloss and transparency, where MgO addition provided more densely crosslinked coatings, probably due to its substantial water solubility resulting

in a considerable concentration of both dissociated metal ions and neutralized carboxylic groups that could be involved in ionic bonding. For reasons of high crosslink density, the latexes synthesized using increased contents of MgO (1, 1.5, and 2 wt % with respect to total monomer feeds) were found to provide highly water whitening resistant coatings. It was also shown that introducing MgO into latexes caused a marked decrease in MFFT due to hydroplasticization of carboxylated emulsion polymer, being more pronounced with the increased content of MgO (transformed predominantly into  $\text{Mg}(\text{OH})_2$ ). With respect to the given facts, it can be concluded that nanostructured MgO represents a promising replacement for ZnO in the role of ionic crosslinker, providing environmentally friendly functional coating binders that could be used as paint binders or clear coats for universal material protection. Taking into account additional significant properties of nanostructured ZnO and MgO, such as antimicrobial activity and ultraviolet absorption, it is highly probable that the reported latex films may provide more desirable qualities than those described in this paper. Further research on these favorable materials is therefore being continued.

**Author Contributions:** Conceptualization, J.M. and A.K.; Methodology, J.M., A.K., J.P. and R.S.; Validation, J.M. and J.Š.; Formal analysis, J.M. and A.K.; Investigation, B.Z., J.P. and R.S.; Writing—original draft preparation, J.M.; Writing—review and editing, J.M. and J.Š.; Visualization, J.M.; Supervision, J.M. and A.K. All authors have read and agreed to the published version of the manuscript.

**Funding:** This research received no external funding.

**Conflicts of Interest:** The authors declare no conflict of interest.

## References

1. Wu, S.; Soucek, M.D. Model compound study for acrylic latex crosslinking reactions with cycloaliphatic epoxides. *J. Coat. Technol.* **1997**, *69*, 43–49. [[CrossRef](#)]
2. Tillet, G.; Boutevin, B.; Ameduri, B. Chemical reactions of polymer crosslinking and post-crosslinking at room temperature. *Prog. Polym. Sci.* **2011**, *36*, 191–217. [[CrossRef](#)]
3. Gonzáles, I.; Asua, J.M.; Leiza, J.R. Crosslinking in acetoacetoxy functional waterborne crosslinkable latexes. *Macromol. Symp.* **2006**, *243*, 53–62. [[CrossRef](#)]
4. Nakayama, Y. Development of novel aqueous coatings which meet the requirements of ecology-conscious society: Novel cross-linking system based on the carbonyl-hydrazide reaction and its applications. *Prog. Org. Coat.* **2004**, *51*, 280–299. [[CrossRef](#)]
5. Li, M.; Lin, X.; Li, X.; Wang, H. Preparation and property study of core-shell ambient-temperature crosslinkable polyacrylate binder. *Appl. Mech. Mat.* **2014**, *469*, 3–6. [[CrossRef](#)]
6. Zhang, S.F.; He, Y.F.; Wang, R.M.; Wu, Z.M.; Song, P.F. Preparation of emulsifier-free acrylate cross-linkable copolymer emulsion and application in coatings for controlling indoor. *Iran Polym. J.* **2013**, *22*, 447–456. [[CrossRef](#)]
7. Koukiotis, C.G.; Karabela, M.M.; Sideridou, I.D. Mechanical properties of films of latexes based on copolymers BA/MMA/DAAM and BA/MMA/VEOVA-10/DAAM and the corresponding self-crosslinked copolymers using the adipic acid dihydrazide as crosslinking agent. *Prog. Org. Coat.* **2012**, *75*, 106–115. [[CrossRef](#)]
8. Koukiotis, C.; Sideridou, I.D. Synthesis and characterization of latexes based on copolymers BA/MMA/DAAM and BA/MMA/VEOVA-10/DAAM and the corresponding 1K crosslinkable binder using the adipic acid dihydrazide as crosslinking agent. *Prog. Org. Coat.* **2010**, *69*, 504–509. [[CrossRef](#)]
9. Zhang, X.; Liu, Y.; Huang, H.; Li, Y.; Chen, H. The diacetone acrylamide crosslinking reaction and its control of core-shell polyacrylate lattices at ambient temperature. *J. Appl. Polym. Sci.* **2012**, *123*, 1822–1832. [[CrossRef](#)]
10. Taylor, J.W.; Winnik, M.A. Functional latex and thermoset latex films. *JCT Res.* **2004**, *1*, 163–190. [[CrossRef](#)]
11. Lee, D.I. The effects of latex coalescence and interfacial crosslinking on the mechanical properties of latex films. *Polymer* **2005**, *46*, 1287–1293. [[CrossRef](#)]
12. Pinprayoon, O.; Saiani, A.; Groves, R.; Saunders, B.R. Particulate ionomer films prepared from dispersions of crosslinked polymer colloids: A structure-property study. *J. Colloid Interface Sci.* **2009**, *336*, 73–81. [[CrossRef](#)]

13. Machotová, J.; Černošková, E.; Honzíček, J.; Šňupárek, J. Water sensitivity of fluorine-containing polyacrylate latex coatings: Effects of crosslinking and ambient drying conditions. *Prog. Org. Coat.* **2018**, *120*, 266–273. [[CrossRef](#)]
14. Schuman, T.; Wikström, M.; Rigdahl, M. Dispersion coating with carboxylated and cross-linked styrene–butadiene lattices. 1. Effect of some polymer characteristics on film properties. *Prog. Org. Coat.* **2004**, *51*, 220–227. [[CrossRef](#)]
15. Kan, C.S.; Blackson, J.H. Effect of Ionomeric Behavior on the viscoelastic properties and morphology of carboxylated latex films. *Macromolecules* **1996**, *29*, 6853–6864. [[CrossRef](#)]
16. Li, J.H.; Hong, R.Y.; Li, M.Y.; Li, H.Z.; Zheng, Y.; Ding, J. Effects of ZnO nanoparticles on the mechanical and antibacterial properties of polyurethane coatings. *Prog. Org. Coat.* **2009**, *64*, 504–509. [[CrossRef](#)]
17. Seo, J.; Jeon, G.; Jang, E.S.; Khan, S.B.; Han, H. Preparation and properties of poly(propylene carbonate) and nanosized ZnO composite films for packaging applications. *J. Appl. Polym. Sci.* **2011**, *122*, 1101–1108. [[CrossRef](#)]
18. Chaurasia, V.; Chand, N.; Bajpai, S.K. Water sorption properties and antimicrobial action of zinc oxide nanoparticles-loaded cellulose acetate films. *J. Macromol. Sci. Pure Appl. Chem.* **2010**, *47*, 309–317. [[CrossRef](#)]
19. Pasquet, J.; Chevalier, Y.; Pelletier, J.; Couval, E.; Bouvier, D.; Bolzinger, M. The contribution of zinc ions to the antimicrobial activity of zinc oxide. *Colloid Surf. A Phys. Eng. Asp.* **2014**, *457*, 263–274. [[CrossRef](#)]
20. Sirelkhatim, A.; Mahmud, S.; Seeni, A.; Kaus, N.H.M.; Ann, L.C.; Bakhori, S.K.M.; Hasan, H.; Mohamad, D. Review on zinc oxide nanoparticles: Antibacterial activity and toxicity mechanism. *Nano-Micro Lett.* **2015**, *7*, 219–242. [[CrossRef](#)]
21. Hong, R.Y.; Li, J.H.; Chen, L.L.; Liu, D.Q.; Li, H.Z.; Zheng, Y.; Ding, J. Synthesis, surface modification and photocatalytic property of ZnO nanoparticles. *Powder Technol.* **2009**, *189*, 426–432. [[CrossRef](#)]
22. Becheri, A.; Dürr, M.; Lo Nostro, P.; Baglioni, P. Synthesis and characterization of zinc oxide nanoparticles: Application to textiles as UV-absorbers. *J. Nanopart. Res.* **2008**, *10*, 679–689. [[CrossRef](#)]
23. Morsi, R.E.; Labena, A.; Khamis, E.A. Core/shell (ZnO/polyacrylamide) nanocomposite: In-situ emulsion polymerization, corrosion inhibition, anti-microbial and anti-biofilm characteristics. *J. Taiwan Inst. Chem. Eng.* **2016**, *63*, 512–522. [[CrossRef](#)]
24. Pan, T.; Lee, Y.; Chu, C.; Chen, Y.; Tsai, C.; Lee, C. Synthesis and characteristics of poly(methacrylic acid-co-Nisopropylacrylamide)/Nano ZnO thermosensitive composite hollow latex particles. *Polymer* **2012**, *53*, 1665–1674. [[CrossRef](#)]
25. Xiong, M.; Gu, G.; You, B.; Wu, L. Preparation and characterization of poly(styrene butylacrylate) latex/nano-ZnO nanocomposites. *J. Appl. Polym. Sci.* **2003**, *90*, 1923–1931. [[CrossRef](#)]
26. Tang, E.; Cheng, G.; Pang, X.; Ma, X.; Xing, F. Synthesis of nano-ZnO/poly(methyl methacrylate) composite microsphere through emulsion polymerization and its UV-shielding property. *Colloid Polym. Sci.* **2006**, *284*, 422–428. [[CrossRef](#)]
27. Tang, E.; Liu, H.; Sun, L.; Zheng, E.; Cheng, G. Fabrication of zinc oxide/poly(styrene) grafted nanocomposite latex and its dispersion. *Eur. Polym. J.* **2007**, *43*, 4210–4218. [[CrossRef](#)]
28. Chimenti, S.; Vega, J.M.; Aguirre, M.; García-Lecina, E.; Díez, J.A.; Grande, H.J.; Paulis, M.; Leiza, J.R. Effective incorporation of ZnO nanoparticles by miniemulsion polymerization in waterborne binders for steel corrosion protection. *J. Coat. Technol. Res.* **2017**, *14*, 829–839. [[CrossRef](#)]
29. Zhu, X.; Zhu, L.; Duan, Z.; Qi, R.; Li, Y.; Lang, Y. Comparative toxicity of several metal oxide nanoparticle aqueous suspensions to Zebrafish (*Danio rerio*) early developmental stage. *J. Environ. Sci. Health A Toxic Hazard. Subst. Environ. Eng.* **2008**, *43*, 278–284. [[CrossRef](#)]
30. Blinova, I.; Ivask, A.; Heinlaan, M.; Mortimer, M.; Kahru, A. Ecotoxicity of nanoparticles of CuO and ZnO in natural water. *Environ. Pollut.* **2010**, *158*, 41–47. [[CrossRef](#)]
31. Abbasalipourkabir, R.; Moradi, H.; Zarei, S.; Asadi, S.; Salehzadeh, A.; Ghafourikhoshroshahi, A.; Mortazavi, M.; Ziamajidi, N. Toxicity of zinc oxide nanoparticles on adult male wistar rats. *Food Chem. Toxicol.* **2015**, *84*, 154–160. [[CrossRef](#)]
32. Sharma, V.; Singh, P.; Pandey, A.K.; Dhawan, A. Induction of oxidative stress, DNA damage and apoptosis in mouse liver after sub-acute oral exposure to zinc oxide nanoparticles. *Mutat. Res.* **2012**, *745*, 84–91. [[CrossRef](#)]

33. Xiao, L.; Liu, C.; Chen, X.; Yang, Z. Zinc oxide nanoparticles induce renal toxicity through reactive oxygen species. *Food Chem. Toxicol.* **2016**, *90*, 76–83. [[CrossRef](#)]
34. Banyal, S.; Malik, P.; Tuli, H.S.; Mukherjee, T.K. Advances in nanotechnology for diagnosis and treatment of tuberculosis. *Curr. Opin. Pulm. Med.* **2013**, *19*, 289–297. [[CrossRef](#)]
35. Sharma, V.; Shukla, R.K.; Saxena, N.; Parmar, D.; Das, M.; Dhawan, A. DNA damaging potential of zinc oxide nanoparticles in human epidermal cells. *Toxicol. Lett.* **2009**, *185*, 211–218. [[CrossRef](#)]
36. Esmaeillou, M.; Moharamnejad, M.; Hsankhani, R.; Tehrani, A.A.; Maadi, H. Toxicity of ZnO nanoparticles in healthy adult mice. *Environ. Toxicol. Pharmacol.* **2013**, *35*, 67–71. [[CrossRef](#)]
37. Boubeta, C.M.; Bacells, L.; Cristofol, R.; Sanfeliu, C.; Rodriguez, E.; Weissleder, R.; Piedrafita, S.; Simeonidis, K.; Angelakeris, M.; Sandiumenge, F.; et al. Self-assembled multifunctional Fe/MgO nanospheres for magnetic resonance imaging and hyperthermia. *Nanomedicine* **2010**, *6*, 362–370. [[CrossRef](#)]
38. Di, D.R.; He, Z.Z.; Sun, Z.Q.; Liu, J. A new nano-cryosurgical modality for tumor treatment using biodegradable MgO nanoparticles. *Nanomedicine* **2012**, *8*, 1233–1241. [[CrossRef](#)]
39. Jin, T.; He, Y. Antibacterial activities of magnesium oxide (MgO) nanoparticles against foodborne pathogens. *J. Nanopart. Res.* **2011**, *13*, 6877–6885. [[CrossRef](#)]
40. Mangalampalli, B.; Dumala, N.; Grover, P. Acute oral toxicity study of magnesium oxide nanoparticles and microparticles in female albino Wistar rats. *Regul. Toxicol. Pharmacol.* **2017**, *90*, 170–184. [[CrossRef](#)]
41. Ghobadian, M.; Nabiuni, M.; Parivar, K.; Fathi, M.; Pazooki, J. Toxic effects of magnesium oxide nanoparticles on early developmental and larval stages of zebrafish (*Danio rerio*). *Ecotoxicol. Environ. Saf.* **2015**, *122*, 260–267. [[CrossRef](#)]
42. Zhang, J.D.; Yang, M.J.; Zhu, Y.R.; Yang, H. Synthesis and characterization of crosslinkable latex with interpenetrating network structure based on polystyrene and polyacrylate. *Polym. Int.* **2006**, *55*, 951–960. [[CrossRef](#)]
43. Kessel, N.; Illsley, D.R.; Keddie, J.L. The diacetone acrylamide crosslinking reaction and its influence on the film formation of an acrylic latex. *J. Coat. Technol. Res.* **2008**, *5*, 285–297. [[CrossRef](#)]
44. Fox, T.G.; Flory, P.J. 2nd-Order transition temperatures and related properties of polystyrene. 1. Influence of molecular weight. *J. Appl. Phys.* **1950**, *21*, 581–591. [[CrossRef](#)]
45. Flory, P.J.; Rehner, J. Statistical mechanics of cross-linked polymer networks II. Swelling. *J. Chem. Phys.* **1943**, *11*, 521–526. [[CrossRef](#)]
46. Tobing, S.; Klein, A. Molecular parameters and their relation to the adhesive performance of acrylic pressure-sensitive adhesives. *J. Appl. Polym. Sci.* **2001**, *79*, 2230–2244. [[CrossRef](#)]
47. Vandenburg, H.J.; Clifford, A.A.; Bartle, K.D.; Carlson, R.E.; Carroll, J.; Newton, I.D. A simple solvent selection method accelerated solvent extraction of additives from polymers. *Analyst* **1999**, *124*, 1707–1710. [[CrossRef](#)]
48. Leitner, J.; Sedmidubský, D. Preparation, properties and utilization of nanostructured ZnO. *Chem. Listy* **2016**, *110*, 406–417.
49. Balducci, G.; Diaz, L.B.; Gregory, D.H. Recent progress in the synthesis of nanostructured magnesium hydroxide. *CrystEngComm* **2017**, *19*, 6067–6084. [[CrossRef](#)]
50. Pi, P.; Wang, W.; Wen, X.; Xu, S.; Cheng, J. Synthesis and characterization of low-temperature self-crosslinkable acrylic emulsion for PE film ink. *Prog. Org. Coat.* **2015**, *81*, 66–71. [[CrossRef](#)]
51. Tsavalas, J.G.; Sundberg, D.C. Hydroplasticization of polymers: Model predictions and application to emulsion polymers. *Langmuir* **2010**, *26*, 6960–6966. [[CrossRef](#)]
52. Jiang, B.; Tsavalas, J.G.; Sundberg, D.C. Water whitening of polymer films: Mechanistic studies and comparison between water and solvent borne films. *Prog. Org. Coat.* **2017**, *105*, 56–66. [[CrossRef](#)]
53. Richard, J.; Maquet, J. Dynamic micromechanical investigations into particle/particle interfaces in latex films. *Polymer* **1992**, *33*, 4164–4173. [[CrossRef](#)]
54. Zosel, A. Mechanical properties of films from polymer lattices. *Polym. Adv. Technol.* **2003**, *6*, 263–269. [[CrossRef](#)]
55. Horský, J.; Quadrat, O.; Porsch, B.; Mrkvičková, L.; Šňupárek, J. Effect of alkalization on carboxylated latices prepared with various amount of a non-ionogenic hydrophilic comonomer 2-hydroxyethyl methacrylate. *Colloids Surf. A Physicochem. Eng. Asp.* **2001**, *180*, 75–85. [[CrossRef](#)]

56. Ruckerova, A.; Machotova, J.; Svoboda, R.; Pukova, K.; Bohacik, P.; Valka, R. Ambient temperature self-crosslinking latices using low generation PAMAM dendrimers as inter-particle crosslinking agents. *Prog. Org. Coat.* **2019**, *119*, 91–98. [[CrossRef](#)]
57. Machotova, J.; Ruckerova, A.; Bohacik, P.; Pukova, K.; Kalendova, A.; Palarcik, J. High-performance one-pack ambient cross-linking latex binders containing low-generation PAMAM dendrimers and ZnO nanoparticles. *J. Coat. Technol. Res.* **2018**, *15*, 1167–1179. [[CrossRef](#)]



© 2020 by the authors. Licensee MDPI, Basel, Switzerland. This article is an open access article distributed under the terms and conditions of the Creative Commons Attribution (CC BY) license (<http://creativecommons.org/licenses/by/4.0/>).